

RESEARCH ARTICLE

10.1002/2013JA019715

Key Points:

- Radio waves are used to find the characteristics of RB electron precipitation
- Storm main phase had large fluxes on the nightside, and dayside fluxes were delayed
- Models of electron precipitation flux and power law spectrum using the Dst index

Correspondence to:

M. A. Clilverd,
macl@bas.ac.uk

Citation:

Simon Wedlund, M., M. A. Clilverd, C. J. Rodger, K. Cresswell-Moorcock, N. Cobbett, P. Breen, D. Danskin, E. Spanswick, and J. V. Rodriguez (2014), A statistical approach to determining energetic outer radiation belt electron precipitation fluxes, *J. Geophys. Res. Space Physics*, 119, 3961–3978, doi:10.1002/2013JA019715.

Received 18 DEC 2013

Accepted 21 APR 2014

Accepted article online 26 APR 2014

Published online 21 MAY 2014

A statistical approach to determining energetic outer radiation belt electron precipitation fluxes

Mea Simon Wedlund¹, Mark A. Clilverd², Craig J. Rodger¹, Kathy Cresswell-Moorcock¹, Neil Cobbett², Paul Breen², Donald Danskin³, Emma Spanswick⁴, and Juan V. Rodriguez^{5,6}

¹Department of Physics, University of Otago, Dunedin, New Zealand, ²British Antarctic Survey, Cambridge, UK,

³Geomagnetic Laboratory, Natural Resources Canada, Ottawa, Ontario, Canada, ⁴Department of Physics and Astronomy, University of Calgary, Calgary, Alberta, Canada, ⁵Cooperative Institute for Research in Environmental Sciences, University of Colorado, Boulder, Colorado, USA, ⁶Also at National Geophysical Data Center, National Oceanic and Atmospheric Administration, Boulder, Colorado, USA

Abstract Subionospheric radio wave data from an Antarctic-Arctic Radiation-Belt (Dynamic) Deposition VLF Atmospheric Research Consortia (AARDDVARK) receiver located in Churchill, Canada, is analyzed to determine the characteristics of electron precipitation into the atmosphere over the range $3 < L < 7$. The study advances previous work by combining signals from two U.S. transmitters from 20 July to 20 August 2010, allowing error estimates of derived electron precipitation fluxes to be calculated, including the application of time-varying electron energy spectral gradients. Electron precipitation observations from the NOAA POES satellites and a ground-based riometer provide intercomparison and context for the AARDDVARK measurements. AARDDVARK radiowave propagation data showed responses suggesting energetic electron precipitation from the outer radiation belt starting 27 July 2010 and lasting ~20 days. The uncertainty in >30 keV precipitation flux determined by the AARDDVARK technique was found to be $\pm 10\%$. Peak >30 keV precipitation fluxes of AARDDVARK-derived precipitation flux during the main and recovery phase of the largest geomagnetic storm, which started on 4 August 2010, were $>10^5$ el cm⁻² s⁻¹ sr⁻¹. The largest fluxes observed by AARDDVARK occurred on the dayside and were delayed by several days from the start of the geomagnetic disturbance. During the main phase of the disturbances, nightside fluxes were dominant. Significant differences in flux estimates between POES, AARDDVARK, and the riometer were found after the main phase of the largest disturbance, with evidence provided to suggest that >700 keV electron precipitation was occurring. Currently the presence of such relativistic electron precipitation introduces some uncertainty in the analysis of AARDDVARK data, given the assumption of a power law electron precipitation spectrum.

1. Introduction

This work builds on the preliminary study undertaken by Clilverd *et al.* [2010a] in which transatlantic VLF radio waves were used to estimate the flux of energetic electrons precipitating into the *D* region of the ionosphere. The great circle subionospheric propagation path from the NAA transmitter in Cutler, Maine, USA, to a receiver in Sodankylä, Finland, provided some estimate of precipitating electron fluxes which had originated from the outer radiation belt ($3 < L < 7$). Obliquely propagating VLF radio waves can be used to monitor electron precipitation through changes in the ionization rate at altitudes of 50–90 km. The excess ionization causes perturbations in the phase and amplitude of the observed signals, which can be readily compared with the nondisturbed quiet day behavior. Through modeling it is possible to determine estimates of the energetic electron precipitation into the atmosphere from the perturbations in the observed signals [e.g., Rodger *et al.*, 2012]. However, Clilverd *et al.* [2010a] identified several limitations in the analysis technique used at the time, particularly in assuming uniform precipitation over the whole propagation path and an unchanging energy spectral gradient of the incident electrons. A further limitation of the analysis was not providing a robust error estimate for the derived fluxes nor a check of the reliability of the electron precipitation flux calculations. This study aims to provide a robust error estimate of derived electron precipitation fluxes and apply time-varying electron energy spectral gradients. This improvement is made possible by using observations of obliquely propagating VLF radio waves from two separate transmitters with nearly identical propagation paths.

Energetic electron precipitation into the atmosphere over $3 < L < 7$ acts as a loss mechanism for the outer radiation belt electron population [Thorne *et al.*, 2005; Meredith *et al.*, 2006; Lam *et al.*, 2010; Morley *et al.*, 2010;

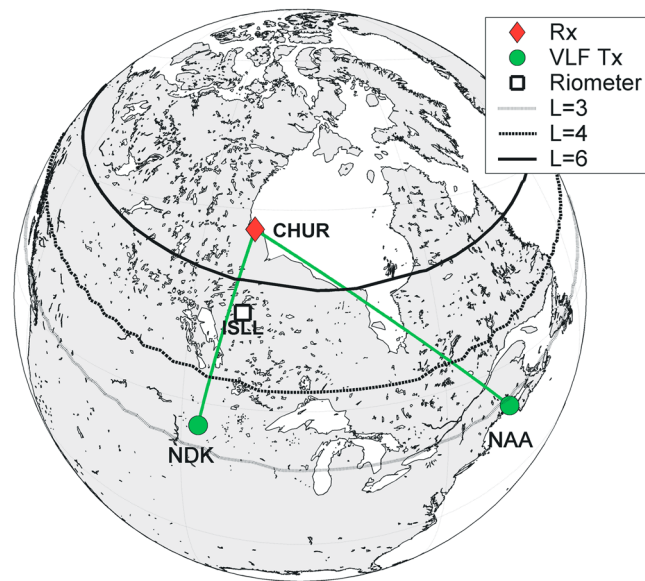


Figure 1. The location of the three subionospheric propagation paths from VLF transmitters NDK, and NAA (circles) to the AARDDVARK receiver site at Churchill (diamond). L shell contours for $L = 3, 4,$ and 6 are shown. The location of the Island Lake riometer is also indicated (square).

Ni et al., 2011; Hendry et al., 2012; Ni et al., 2013] and as an indicator of the mechanisms taking place inside the belt [*Li et al., 2013*]. Through a complex interplay between the acceleration, transport, and loss of electrons, individual geomagnetic storms can drive large changes in the flux of relativistic electrons within the outer radiation belts [*Reeves et al., 2003*], potentially damaging satellites [*Allen, 2010; Clilverd et al., 2012*], disrupting power grids, and endangering astronauts. An example of a period of enhanced geomagnetic activity, which induced changes in the radiation belt environment through enhancing relativistic electron fluxes is July–August 2010. This period has been partially analyzed by *Lichtenberger et al. [2013]*, especially in terms of changes to the underlying cold plasma structures, including the

movement of the plasmapause. Using the technique of *Clilverd et al. [2010a]*, we can investigate the causes of electron precipitation throughout the period of disturbance and determine the precipitation fluxes involved.

In this study we analyze data from an Antarctic-Arctic Radiation-Belt Dynamic Deposition VLF Atmospheric Research Consortia (AARDDVARK) network receiver located in Churchill, Canada, and concentrate on signals from two U.S. transmitters (call signs NAA and NDK). The AARDDVARK network provides continuous long-range observations of the lower ionosphere [*Clilverd et al., 2009*]. The Consortia sensors detect changes in ionization levels from ~ 30 to 85 km altitude, with the goal of increasing the understanding of energy coupling between the Earth's atmosphere, Sun, and space. We use the upper atmosphere as a gigantic energetic particle detector to observe and understand changing energy flows. The signals are used in this study to determine the effects of electron precipitation into the atmosphere over the range $3 < L < 7$, i.e., where outer radiation belt processes occur. We aim to address the limitations of the previous analysis by *Clilverd et al. [2010a]* through additional modeling efforts and by combining the AARDDVARK data from the two paths. Both of these paths are relatively short, leading to less complex local time variability along the path. In addition, the two transmitters are very similar in frequency such that there should be similar perturbation responses to electron precipitation, and their geomagnetic latitudes are also very similar so there will be a similar variation of electron precipitation along each path. As such, we combine the data from the two transmitters in order to confirm estimated fluxes, calculate the error bars, and intercompare the results.

We also compare the results from the AARDDVARK network with fluxes from the NOAA POES satellite, and a ground-based riometer. The AARDDVARK observations used in this study have the advantage of integrating the electron precipitation effects over the whole of the magnetic footprint of the outer radiation belt, using the atmosphere as a detector of all incident particles. In comparison, the riometer only makes a point measurement and may be subject to small-scale variability, and the POES detectors have a restricted capacity to measure all of the electron population in the bounce-loss-cone [see *Rodger et al. [2010a]* for a comprehensive review of the POES satellite detector characteristics].

2. Experimental Setup

To study the energetic electron precipitation fluxes into the atmosphere during the July–August 2010 period we use narrow band subionospheric very low frequency (VLF) data spanning 24–25 kHz received at Churchill, Canada (geographic $58^{\circ}44'N, 93^{\circ}49'W, L = 7.6$). The Churchill site is part of the AARDDVARK network

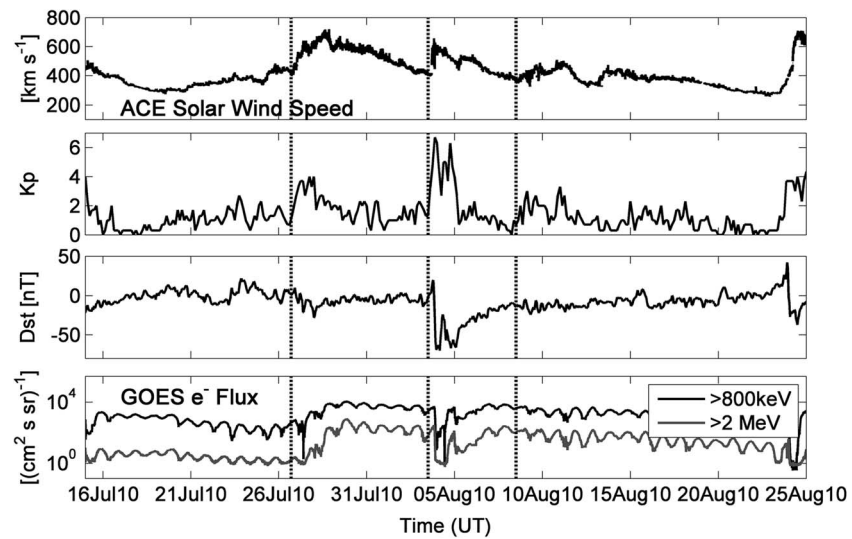


Figure 2. Geomagnetic conditions over July–August 2010. The daily solar wind speed, Kp , Dst , GOES > 0.8 MeV and > 2 MeV electron fluxes are plotted in separate panels. The start of three periods of solar wind and geomagnetic disturbance are identified by vertical dotted lines. Initially, a small enhancement in geomagnetic activity is seen on 26 July, following an increase in solar wind speed, after which the GOES > 0.8 MeV and > 2 MeV fluxes are elevated for some days.

([Clilverd *et al.*, 2009]; for further information see the description of the array at www.physics.otago.ac.nz/space/AARDDVARK_homepage.htm). The transmitters studied have call signs NAA (24.0 kHz, geographic $44^{\circ}39'N$, $67^{\circ}17'W$, $L = 2.9$), and NDK (25.2 kHz, geographic $46^{\circ}22'N$, $98^{\circ}20'W$, $L = 3.2$). Figure 1 shows the location of the Churchill radio wave receiver site (diamond) and the transmitter-receiver paths that are studied during the event period (NAA and NDK transmitter locations are shown by the circles). The propagation paths span the range $3 < L < 7$, effectively integrating the subionospheric electron precipitation along the paths from the whole of the outer radiation belt.

Figure 2 shows the geomagnetic and radiation belt conditions during the 20 July to 22 August 2010 period that is studied in this paper. The solar wind speed, Kp , Dst , and GOES 11 > 0.8 and > 2 MeV electron flux are plotted in separate panels, ordered from top to bottom. (The GOES 11 > 0.8 MeV fluxes are corrected using a recalibrated geometrical factor [e.g., Gannon *et al.*, 2012].) The start of three periods of solar wind and geomagnetic disturbance are identified by vertical dotted lines. The solar wind speed ranged from 250 km s^{-1} to 700 km s^{-1} . Overall the solar wind was consistently above 400 km s^{-1} from 26 July to 15 August 2010. The first small geomagnetic disturbance occurred on 27 July 2010, with Kp varying between 2 and 4, but with no obvious storm signature in Dst . However, the GOES 11 > 0.8 and > 2.0 MeV trapped electron fluxes increased by 2 orders of magnitude shortly after the disturbance and remained elevated for several days afterward. The GOES 11 data are consistent with a radiation belt electron acceleration event on 27 July, caused by the arrival of a corotating interaction region (CIR) under otherwise quiet conditions and then a shock arrival on 3 August that caused a dropout in the relativistic electron fluxes followed by a recovery to the prior levels. Characteristic changes in solar wind properties across the stream interface in the 27 July CIR (flow speed and temperature increases, density decrease, elevated magnetic field magnitude, and a shift in the azimuthal velocity from negative to positive [Gosling *et al.*, 1978]) were observed by Wind. As time shifted in the OMNI data, this stream interface reached the Earth ~ 0200 UT on 27 July. Following a brief dropout, the GOES 11 > 0.8 and > 2 MeV trapped fluxes started to recover about 10 h later, consistent with expected radiation belt behavior after the passage of a CIR [Borovsky and Denton, 2009] and in fact increased 2 orders of magnitude over the pre-CIR levels. The solar wind speed enhancement associated with the first disturbance, a gradual increase over several days consistent with a high-speed stream following the CIR, reached the highest levels in the study period at $\sim 700 \text{ km s}^{-1}$ on 28 July. Several days after the 27 July CIR, in a complex series of events that has received much attention [Möstl *et al.*, 2012, and references therein], several coronal mass ejections (CMEs) were launched in rapid succession on 1 August. A shock was observed by Wind at L1 following the first

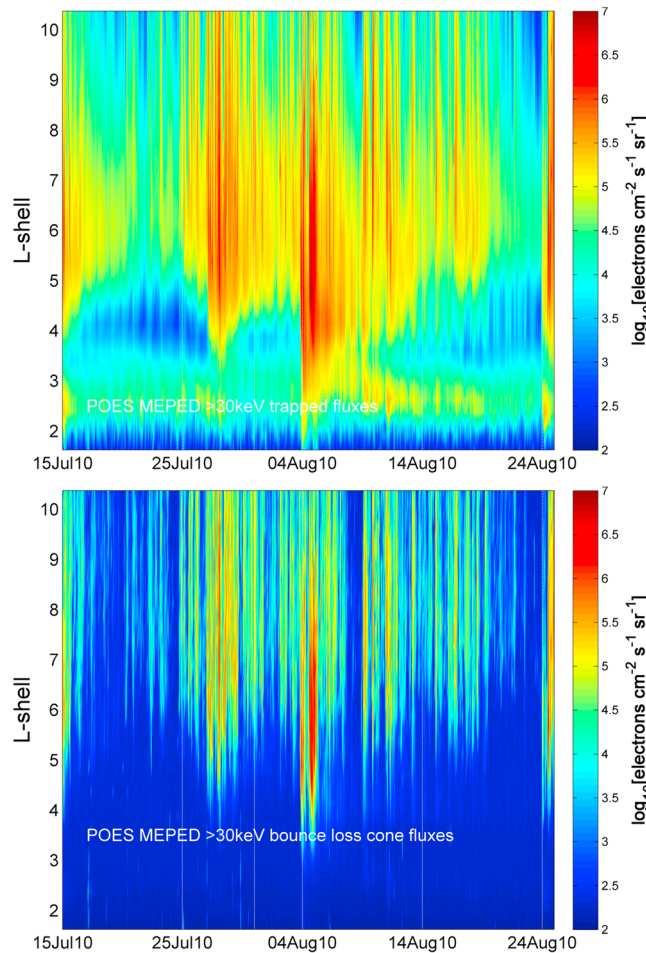


Figure 3. The zonally averaged >30 keV POES (top) trapped and (bottom) precipitating electron fluxes during the study period in July/August 2010. The *L* shell ranges cover the inner and outer radiation belts, where several enhancements in flux occur. Color scales represent Log_{10} of electron flux ($\text{cm}^{-2} \text{s}^{-1} \text{sr}^{-1}$).

the period 9–12 August 2010, where *Kp* was slightly elevated ($2 < Kp < 4$), and the solar wind was also slightly elevated ($>400 \text{ km s}^{-1}$).

In this study we also make use of particle measurements by the Space Environment Monitor-2 instrument package onboard the POES spacecraft which are in Sun-synchronous orbits at ~800–850 km altitudes [Evans and Greer, 2004]. SEM-2 includes the Medium Energy Proton and Electron Detector (MEPED), in addition to the Total Energy Detector (TED). Together these instruments monitor electron fluxes from 50 eV up to 2700 keV. The 0°-pointing detectors are mounted on the three-axis stabilized POES spacecraft so that the center of each detector field of view is outward along the local zenith, parallel to the Earth-center-to-satellite radial vector. Another set of detectors, termed the 90° detectors, are mounted approximately perpendicular to the 0° detector. In addition, there is also a set of omnidirectional measurements made from a dome detector which is mounted parallel to the 0° detectors. The detectors pointing in the 0° and 90° directions are ±15° wide, while the omnidirectional dome detectors (termed “omni”) are ±60° wide. Modeling has been used to determine the radiation belt populations monitored by the telescopes [Rodger et al., 2010a, 2010b]. For the *L* shells that we consider the 90°-detector appears to primarily respond to trapped electrons, and hence we will refer to it as the “trapped detector”. In contrast, the 0°-detector views inside the bounce loss cone (BLC), and is measuring some fraction of the precipitating electron population. Hence we will refer to it as the “precipitating detector.” In Figure 3 we show the >30 keV POES (top) trapped and (bottom) precipitating electron fluxes as a function of *L* shell during the study period. The proton contamination has been

and ahead of the second of the ejecta, and a narrow, very high density region was observed ahead of the third of the ejecta [Möstl et al., 2012]. An energetic storm particle event [Cohen, 2006] that was too weak in >10 MeV solar proton fluxes to trigger a NOAA Solar Radiation Storm alert was associated with this shock. Storm sudden commencements (SSCs) [Curto et al., 2007] resulting from the arrivals of the shock and of the very high-density region were identified at 1740 UT on 3 August and at 1018 UT on 4 August. The resulting geomagnetic disturbance was characterized by a moderate magnetic storm response in *Dst* (minimum *Dst* ~ -60 nT) and a maximum *Kp* of 7-. After the first SSC, the GOES 11 relativistic electron fluxes underwent a 2 order-of-magnitude dropout, followed by a recovery interrupted by a brief dropout after the second SSC. The trapped fluxes recovered to preshock levels after 3 days, then gradually decreased until another dropout on 23–24 August. A third period of disturbance is identified here as

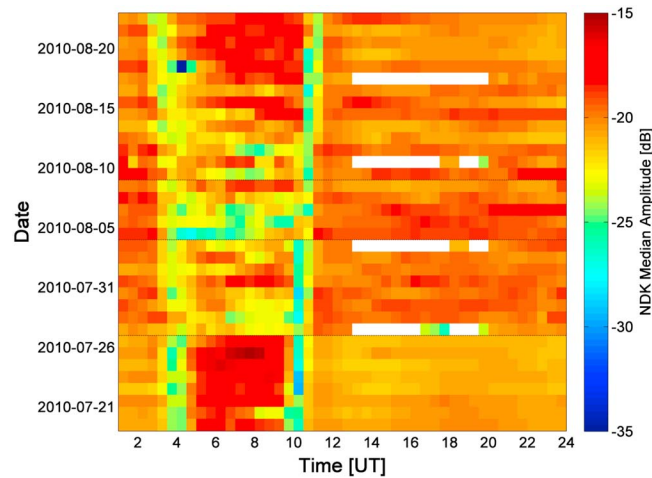


Figure 4. Median amplitude variations of the NDK transmitter received at Churchill from 20 July 2010 until 23 August 2010. The color scale is in decibel relative to an arbitrary voltage. Horizontal dashed lines represent significant changes in the behavior of the data on 27 July, 4, and 9 August 2010, where nighttime (03–10 UT) amplitudes change from ~ -17 dB to < -20 dB and daytime amplitudes (12–24 UT) increase from -22 dB to ~ -20 dB. White shading represents transmitter off periods.

that intersect the subionospheric great circle paths from the transmitters NDK and NAA to the AARDDVARK receiver at Churchill.

3. Results

3.1. Amplitude Behavior

Median amplitude variations of the NDK transmitter received at Churchill from 20 July 2010 until 23 August 2010 are shown in Figure 4. Four separate regimes can be seen in the data, with daytime propagation conditions from 12 to 03 UT (06–21 LT), nighttime propagation conditions from 05 to 10 UT (23–04 LT), sunset from 03 to 05 UT (21–23 LT), and sunrise from 10 to 12 UT (04–06 LT). Horizontal dashed lines represent significant changes in the behavior of the data on 27 July 2010 and 4 August 2010, where nighttime amplitudes change from about -17 dB to less than -20 dB (red to yellow) and daytime amplitudes increase from -22 dB to about -20 dB (yellow to orange). Although smaller than nighttime amplitude changes, the daytime changes are still very significant in terms of electron precipitation fluxes, as will be shown later in the paper. Decreases in nighttime amplitudes and increases in daytime amplitudes are consistent with the observations of storm time behavior in *Clilverd et al.* [2010b]. The nighttime observations in Figure 4 particularly show that electron precipitation occurs into the atmosphere monitored by this path from 27 July until about 16 August, i.e., for more than 2 weeks. In this data set the period prior to the first small geomagnetic disturbance on 27 July can be considered as a “quiet day”, i.e., unaffected by electron precipitation or other *D* region disturbances which affect the AARDDVARK observations. By 20 August, similarly quiet conditions can also be seen. During the study period, there were three very weak solar proton events (on 3, 14, and 18 August 2010) adding to the ionization impacting on the high-latitude ionosphere. The first is the energetic storm particle event mentioned earlier. The most intense of these in the >10 MeV fluxes that occurred at 1230 UT on 14 August 2010, with a peak flux of only 14 protons \cdot s $^{-1}$ sr $^{-1}$ cm $^{-2}$ (proton flux units or pfu) for >10 MeV protons measured at geostationary orbit.

3.2. Amplitude Error Bars

The quiet day diurnal variation of the NDK-Churchill amplitude for 5 days, 22–26 July 2010 inclusive are shown in Figure 5. The mean (blue dot) and median (black dot, red line) quiet day curve for NDK-Churchill is plotted, with a half-hourly error bar representing a 95% confidence interval (\pm error) for the median. For each 30 min period within a day’s data, we define our sample set as the 1 min resolution data points within that time period. We use the central limit theorem of statistics to find the median of the amplitude

removed using the algorithm given in *Lam et al.* [2010, Appendix A], which has been described in more detail in a recent NOAA Technical Report [Green, 2013]. The International Geomagnetic Reference Field model was used to compute the *L* shell and was performed by NOAA as part of the basic POES data set. Several enhancements in flux can be seen, both in the trapped and the precipitating fluxes. The precipitating fluxes range from *L* \sim 5–9 during the event, which starts on 27 July 2010, and from *L* \sim 4–10 during the event that starts on 4 August 2010. As such there is a significant zone of electron precipitation that is observed to occur on *L* shells

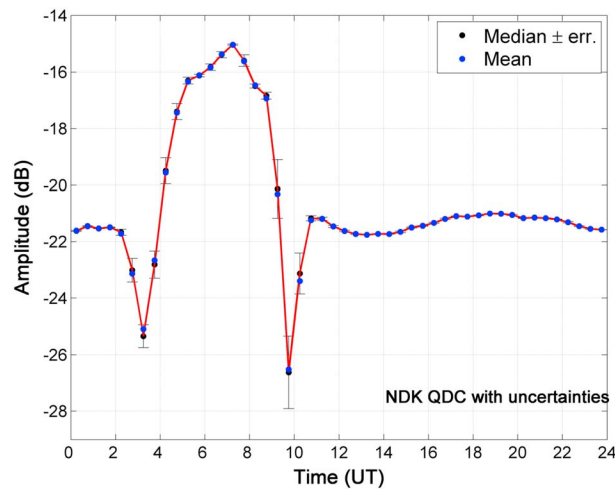


Figure 5. The quiet day diurnal variation in the NDK-Churchill amplitude for 5 days, 22–26 July 2010 inclusive. Also shown are half hourly mean (blue dot) and median (black dot, red line) values, with an error bar representing the 95% confidence interval of the median. The mean and median are usually over plotted on each other and hard to distinguish.

values in a time period as a representative value for that period. We estimate the error of a time period by bootstrapping a 95% confidence interval for the median. A bootstrapped confidence interval for a median is found by the data set being resampled with replacement (to the same number of items as the set) a certain number of times (we used 1000 times), and the median is calculated on each sample. These calculated medians are then used as a distribution to find the interval within which we are 95% confident that the true median value lies. We take the error as half of the range of the confidence interval. We also apply the same approach for determining the parameters for each time zone, such that the amplitude

for the zone can be described by a single representative median value and error. In the same way, we determine these values for the quiet day curve, for both 30 min time periods and each time zone. The error in the hardware and software of the experiment itself, which we determined to be ± 0.015 dB, applies to the raw data and is effectively removed by the preprocessing of data to 1 min median values prior to our analysis. To compare a time period in a day with the same period in the quiet day curve, we find the absolute value of the difference between the two representative median amplitude values, with the uncertainty defined through the error as $err_{total} = (err_{QDC}^2 + err_{Day}^2)^{1/2}$ for each 30 min time period or time zone.

Typically, the quiet daytime amplitudes are quite repeatable, being controlled primarily by daytime solar UV levels [e.g., *McRae and Thomson, 2000*] and thus have a small error ($err = 0.03$ dB). The quiet nighttime amplitudes show more variability as a result of more complex propagation conditions at night associated with a less well defined lower ionosphere [*Thomson et al., 2007*]. Nighttime error values are therefore typically larger than daytime (0.15 dB cf. 0.03 dB). As discussed in *Ciliverd et al. [2010a]*, deviations from the quiet day curve, being caused by additional ionization from electron precipitation, are often observed as decreases in amplitude during the night and increases in amplitude during the day. Thus, to generate the quiet day curve, we have used the upper/lower envelope exhibited during the five quiet days.

Given the changing propagation conditions throughout the nondisturbed day, we can break it into specific local time zones with individual propagation characteristics. Figure 6 shows two representative days showing the absolute amplitude perturbation from the quiet day curve of NAA-Churchill. The days are 24 (Figure 6, top) and 28 (Figure 6, bottom) July 2010. The panels show how each day is broken up to six zones, such as day (zones I and VI), night (zone III), sunset (zone II), sunrise (zone IV), and also periods where transmitter maintenance might affect the daytime data (zone V). Each panel shows the absolute amplitude perturbation of NAA signals received at Churchill. Half-hourly median and error bars are shown (black symbols), as well as mean, median, and error bars for each zone (red symbols). The data from 24 July 2010 represent one of the quiet days, and, therefore, the resultant perturbation values are close to zero, with small errors (except during sunset when changing propagation conditions lead to high variability and hence a large uncertainty in zone II). The data from 28 July 2010 represent a disturbed day and show significant perturbation levels in all of the zones.

Figure 7 shows the absolute amplitude perturbation for NDK-Churchill and NAA-Churchill during the study period (20 July to 22 August 2010), concentrating on the results from three of the zones identified in Figure 6. Zone III (blue line) represents the nighttime, i.e., 00 MLT, zone V (purple line) represents the daytime (10 MLT). Occasionally transmitter off periods affect the zone V data, so zone VI (green line) can be used to represent the daytime instead (16 MLT), but the zones should be very similar for times when transmitter off

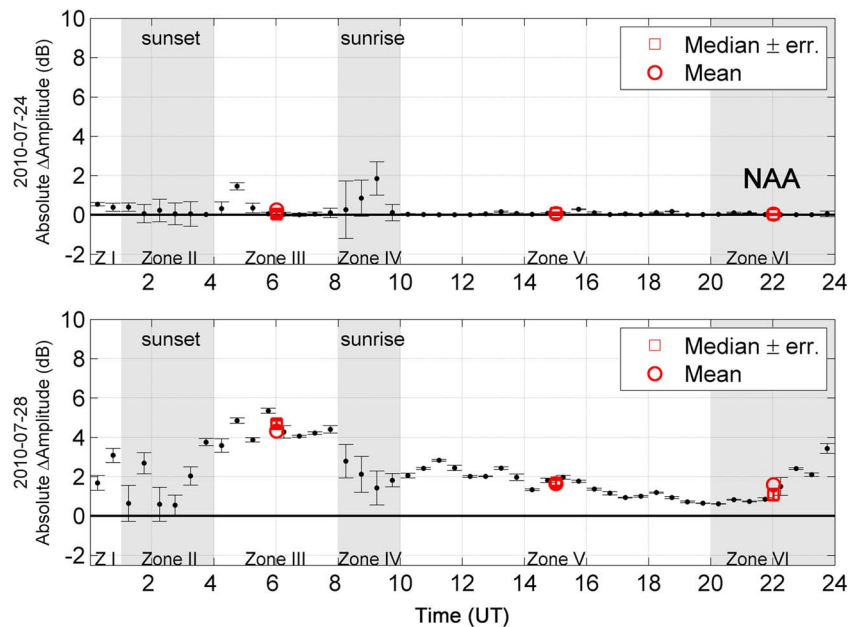


Figure 6. Two representative days showing the absolute amplitude perturbation to the quiet day curve of NAA-Churchill. (top) The prestorm diurnal absolute amplitude perturbation of NAA signals received at Churchill during 24 July 2010. The day is broken into six local time zones, such as day (zones I and VI), night (zone III), sunset (zone II), sunrise (zone IV), and also periods where transmitter maintenance might affect the daytime data (zone V). At Churchill LT = UT – 6. Half hourly error bars, plus LT zone mean, and median values are plotted. (bottom) The same as Figure 6 (top), but for a more perturbed day, 28 July 2010.

periods are not occurring, as confirmed in this figure. Transmitter off times are usually caused by weekly maintenance periods, which generally occur during a specific day of the week (different for different transmitters) and at set times—thus, we can identify the periods affected and remove them from the analysis. In subsequent plots we use this approach to represent the daytime data. Error bars for the values for each time zone are shown. Enhancements in the perturbation level can be seen from 27 July 2010, lasting until 31 July, and then again on 4 August, lasting about 8 days. In the figure, the start of the disturbance periods are denoted by a storm symbol (black star).

In terms of absolute amplitude perturbation level, the nighttime shows much larger effects than either of the daytime zones, for both NDK and NAA. However, the daytime zones show similar patterns of perturbation compared with the nighttime and respond to both of the geomagnetic disturbances. As before, the daytime error values are usually smaller than the nighttime ones, with typically ± 0.07 dB compared with ± 0.16 dB. Comparing the NDK nighttime perturbation variation with the NAA nighttime perturbation variation shows that NDK amplitude changes are largest during the storm period, while NAA changes peak after the storm period. In the next section we undertake to model the amplitude perturbation for nighttime and daytime as a function of electron precipitation flux and hence convert the perturbation values observed into more meaningful measurements.

4. Electron Precipitation Flux From NDK and NAA-Churchill Amplitudes

Here we use a very similar method to that described in *Clilverd et al.* [2010a] and updated in *Rodger et al.* [2012]. For completeness we summarize the technique here. The VLF wave propagation of NDK or NAA to Churchill is calculated using the Long Wave Propagation Code (LWPC) [Ferguson and Snyder, 1990], which models VLF signal propagation from any point on Earth to any other point. The upper boundary condition, provided by the D region electron density altitude profile, is often expressed through a Wait ionosphere. The electron number density (i.e., electrons per cubic meter), N_e , increases exponentially with altitude z and is defined in terms of a sharpness parameter β and a reference height h' [Wait and Spies, 1964]. To model the perturbation we assume that the whole path is affected by excess ionization in the energy range 10 keV–3 MeV, which is inputted into an underlying “ambient” ionosphere. The β and h' of the ambient ionosphere

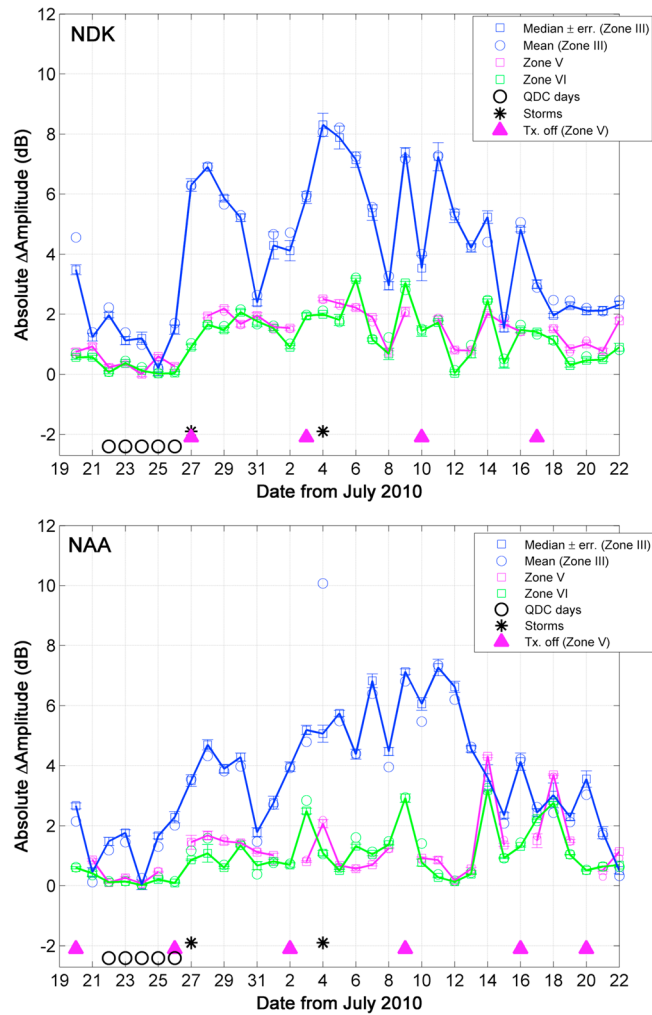


Figure 7. The variation in absolute amplitude perturbation for NDK-Churchill and NAA-Churchill for 20 July to 22 August 2010. The results from three local time zones are plotted, zone III (night, blue line), zone V (day, purple line), and zone VI (day, green line). Error bars for the values for each time zone are shown. Storm onsets on 27 July 2010 and 4 August are denoted by black stars. Transmitter off periods are identified by purple triangles.

are provided by the analysis of *McRae and Thomson [2000]*, *Thomson and McRae [2009]*, and *Thomson et al. [2011]* depending on local time being modeled, while the electron number density at higher altitudes is provided by the International Reference Ionosphere (IRI-2007) from http://omniweb.gsfc.nasa.gov/vitmo/iri_vitmo.html.

The background neutral atmosphere is calculated using the NRLMSISE-00 neutral atmospheric model [*Picone et al., 2002*]. We then use a model to describe the balance of electron number density in the lower ionosphere, based on that given by *Rodger et al. [1998]* and updated in *Rodger et al. [2007]* and *Rodger et al. [2012]*. In this model the evolution of the electron density in time is governed by the equation

$$\frac{\partial N_e}{\partial t} = q - \beta N_e - \alpha N_e^2$$

where q is the ionization rate, α is the recombination coefficient ($\text{m}^3 \text{s}^{-1}$), and β is the attachment rate (s^{-1}).

In addition to the background ionization, we also calculate the excess ionization generated by electron precipitation. The ionization rate due to precipitating energetic electrons is calculated by an application of the expressions in *Rees [1989]*, expanded to higher energies based on *Goldberg and Jackman [1984]*. The equations used are fully specified in *Rodger et al. [2002, section 2.2]* and are thus not reproduced in detail here.

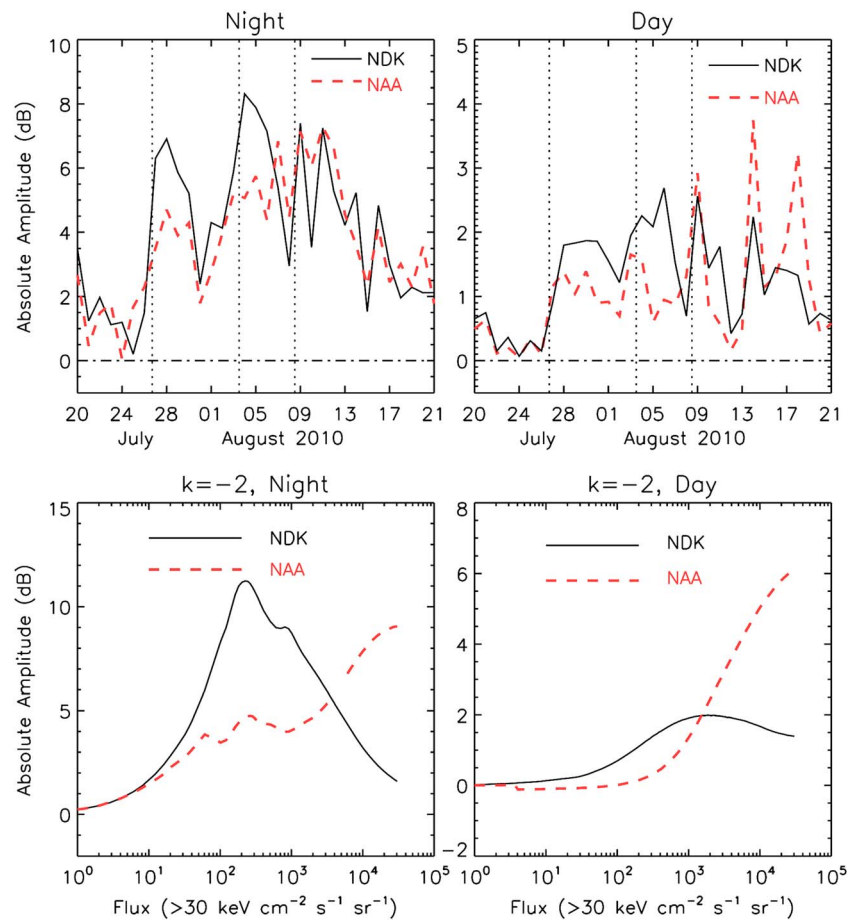


Figure 8. (top) Night and day variations in NAA (dashed line) and NDK (solid line) absolute amplitude perturbations from 20 July to 21 August 2010. Vertical dashed lines indicate the start and end of enhanced geomagnetic activity. Data for the night panel are taken from Zone III, while data for the day panel are taken from Zone V and Zone VI in order to compensate for transmitter off periods during some of the days. (bottom) calculated night and day perturbations of NAA (dashed line) and NDK (solid line) as a function of precipitation flux with spectral gradient $k = -2$.

We assume a spectral gradient varying with a power law scaling exponent (which we describe using the parameter k), and thus the electron flux (F) is related to the electron energy (E) by a power law. This assumption is supported by the analysis of Whittaker *et al.* [2013], which showed that for electron precipitation energies >70 keV, power law gradients were a more accurate description of the energy spectrum than either e -folding or kappa type fits.

The electron number density profiles determined for varying precipitation flux magnitudes and varying k are used as input to the LWPC subionospheric propagation model, thus modeling the perturbation of NDK received at Churchill. Similar analysis is done for NAA received at Churchill.

Figure 8 shows the experimentally observed absolute amplitude perturbations for both NDK and NAA for nighttime (top left) and daytime (top right). Vertical dashed lines indicate the start, intensification, and end of enhanced geomagnetic activity. Overall, there appear to be two periods which show distinctly different behavior patterns of the two transmitters. The nighttime period from 27 July to 7 August 2010 NDK (solid line) exhibits a substantially larger perturbation level compared with NAA (dashed line). However, after 7 August, the perturbation levels are very similar for both transmitters. In both periods the perturbations are large (~ 5 dB).

On the right hand side of Figure 8, the daytime period is shown. The daytime NDK perturbations from 27 July to 7 August 2010 are slightly larger than those of NAA. After 7 August, the daytime NAA perturbations are initially similar to NDK and then substantially larger than NDK. As described above, the daytime perturbation

data are made up of an average of zone V and zone VI values, in order to compensate for transmitter off periods which typically occur once a week, in zone V.

The bottom panels of Figure 8 provide an example of how the calculated amplitude perturbation of NDK (solid line) and NAA (dashed line) varies as the >30 keV electron precipitation flux increases from 10^0 to 10^5 el $\text{cm}^{-2} \text{s}^{-1} \text{sr}^{-1}$ with a spectral gradient power law scaling exponent set at $k = -2$. This $k = -2$ value was used in *Clilverd et al.* [2010a], but in that paper it was noted that it could vary by ± 1 , and we take that variation into account further in this analysis. Figure 8, left shows the amplitude variation for nighttime propagation conditions and Figure 8, right shows the daytime situation. The panels give potential insight into the different responses observed during the July–August 2010 geomagnetic disturbances. For example, when the >30 keV precipitating electron flux is 10^2 – 10^3 el $\text{cm}^{-2} \text{s}^{-1} \text{sr}^{-1}$ during the nighttime, NDK shows a significantly larger absolute amplitude perturbation than NAA (10 dB cf. 5 dB). However, when the >30 keV precipitating electron flux is $\sim 10^1$ el $\text{cm}^{-2} \text{s}^{-1} \text{sr}^{-1}$ during the nighttime, NDK has a similar perturbation level to NAA, as observed (~ 2 dB). After 7 August 2010, both NDK and NAA sometimes show absolute amplitude perturbations that are about equal and in the range 4–8 dB. The modeling results using $k = -2$ suggest that the >30 keV flux would need to be $\sim 3 \times 10^3$ el $\text{cm}^{-2} \text{s}^{-1} \text{sr}^{-1}$ in order to reproduce these observations. Thus, during the period 27 July to 7 August 2010, the nighttime precipitation fluxes appear to be slightly lower than during the period after 7 August. However, this interpretation would be different for non- $k = -2$ spectra. From this simple analysis of the amplitude perturbations, it is clear that an understanding of the spectral gradient is important in deriving the final fluxes.

The daytime perturbations observed on NDK are also found to be slightly larger than those on NAA in the period 27 July to 7 August 2010 (~ 2 dB for NDK cf. ~ 1 dB for NAA). The daytime calculations for $k = -2$ (bottom right) suggest that the observations from both transmitters can be explained by a >30 keV electron precipitation flux of 10^2 – 10^3 el $\text{cm}^{-2} \text{s}^{-1} \text{sr}^{-1}$. After 7 August, the NAA daytime perturbations are sometimes larger than those on NDK. The $k = -2$ model calculations indicate that this occurs when the >30 keV electron fluxes are larger than those during the 27 July to 7 August disturbance period. NAA perturbation values of ~ 3 dB and NDK ~ 1.5 dB suggests daytime fluxes of 5×10^3 el $\text{cm}^{-2} \text{s}^{-1} \text{sr}^{-1}$ in this later time period.

One parameter that strongly influences the calculated fluxes is the value of power law scaling exponent used to describe the electron precipitation energy spectrum. We can model the effect of changing the scaling component and calculate the fluxes during the study period using the perturbation levels on each individual transmitter, as well as the relative differences. Using the relationship between the perturbation in the amplitude of NAA and NDK, it is possible to determine the spectral gradient for each time zone and for each day. By knowing the perturbation amplitude on NAA and NDK for any given time, we can look up the corresponding values from the modeling resulting from different spectral gradient conditions (i.e., $k = -1, -1.5, -2, -2.5, 3$, etc.) and assign a spectral value to that time.

By combining the perturbation levels in NAA and NDK received at Churchill, with the LWPC modeling results, we are able to determine the electron precipitation fluxes for daytime and nighttime conditions, taking into account varying spectral gradients. The precipitation fluxes are shown in Figure 9 (top) which shows the night (black) and day (red) $3 < L < 7 > 30$ keV precipitating electron flux variation during the study period. Electron fluxes are enhanced following the initial small geomagnetic disturbance on 27 July until about 17 August. The highest calculated fluxes were $\sim 10^6$ el $\text{cm}^{-2} \text{s}^{-1} \text{sr}^{-1}$, occurring several days after the largest geomagnetic disturbance in the study period, which began on 3 August 2010. The daytime electron fluxes are consistently larger than the nighttime fluxes, apart from during the onset of the geomagnetic disturbances on 27 July and 3 August 2010. The error bars for daytime are about the same nighttime fluxes, which is simply a consequence of the sensitivity of the LWPC modeling results to small changes in amplitude during the day. As we discussed earlier, the nighttime amplitude values exhibit larger error values than the daytime values do, but this is not translated into larger precipitating flux variations. From 9 August 2010, precipitating electron fluxes are generally lower than those during the largest geomagnetic disturbance period, but there are times when large fluxes are present, i.e., daytime on 9 and 14 August and nighttime on 10 and 13 August.

Figure 9 (middle) shows the daily $3 < L < 7$ geometric mean of the >30 keV trapped and BLC electron flux for zonally averaged POES data (solid black line), the >30 keV BLC electron flux (dashed black line), and the day-night averaged AARDDVARK > 30 keV flux (red). We show the geometric mean of the trapped and BLC POES fluxes following the work of *Hargreaves et al.* [2010] and *Rodger et al.* [2013], who showed that >30 keV fluxes

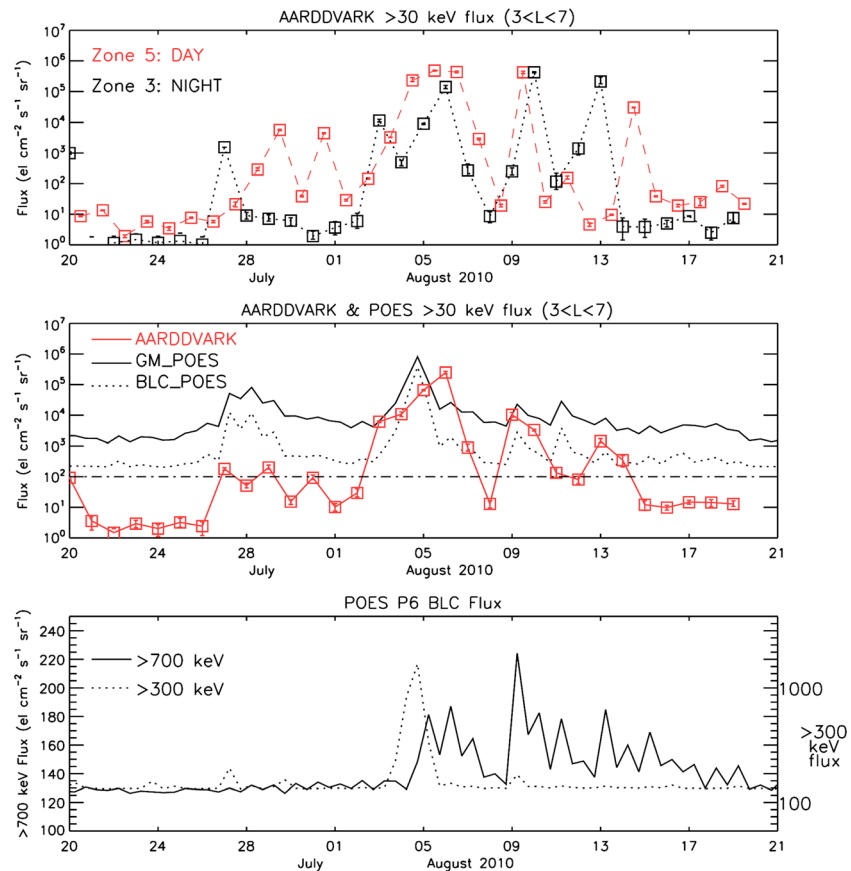


Figure 9. (top) AARDDVARK $3 < L < 7 > 30$ keV daytime (red) and nighttime (black) fluxes during the study period. (middle) POES $3 < L < 7 > 30$ keV zonally averaged geometric mean of the trapped and precipitating flux (GM_POES, black solid line), POES $3 < L < 7 > 30$ keV zonally averaged BLC flux (BLC_POES, black dashed line), and the daily averaged AARDDVARK >30 keV electron flux (red). The dash-dotted horizontal line represents the lower noise floor of the POES electron detectors. (bottom) POES $3 < L < 7 > 700$ keV zonally averaged BLC flux.

determined from Finnish riometer absorption observations during POES overflights was best described by the geometric mean of trapped and BLC POES fluxes, rather than BLC fluxes alone. The plot shows us that during the period of highest fluxes (5 August 2010), there is reasonable agreement between all three data series, with the geometric mean flux and the BLC flux from POES only differing by a factor of ~ 2 at the peak and the AARDDVARK fluxes spanning both within its error bar. However, during the rest of the study period, the AARDDVARK fluxes tend to be lowest and the POES BLC fluxes are typically higher than the AARDDVARK fluxes but not as high as the geometric mean fluxes. In a significant proportion of the study period, the POES fluxes appear to be close to the lower sensitivity limit of the BLC instrument, i.e., $\sim 10^2$ $\text{el cm}^{-2} \text{s}^{-1} \text{sr}^{-1}$ for the BLC detector and $\sim 10^3$ $\text{el cm}^{-2} \text{s}^{-1} \text{sr}^{-1}$ for the geometric means. The AARDDVARK fluxes exhibit a variation of 6 orders of magnitude over the study period, while the BLC fluxes show 4 orders of magnitude and the geometric mean fluxes only 3. Primarily, the smaller ranges exhibited by the POES fluxes is due to the background level sensitivity limit, and in practice the fluxes could be anything at or below that level. This suggests that while *Hargreaves et al.* [2010] and *Rodger et al.* [2013] indicate that the geometric mean works well to describe the peak energetic electron precipitation fluxes for events occurring above Kilpisjärvi, Figure 9 suggests that it does not work well during geomagnetically quiet periods.

During the small geomagnetic disturbance of 27 July 2010, the POES >30 keV BLC fluxes are higher than the equivalent AARDDVARK fluxes, and during the main phase of the large disturbance (3–5 August), the fluxes are similar. However, following the large geomagnetic disturbance, there are occasions where the AARDDVARK fluxes are higher than the POES BLC fluxes, as shown in Figure 9 (middle), occurring on 6, 9, 10, and 13 August. Because the AARDDVARK technique is dependent on obliquely propagating subionospheric VLF waves, it is

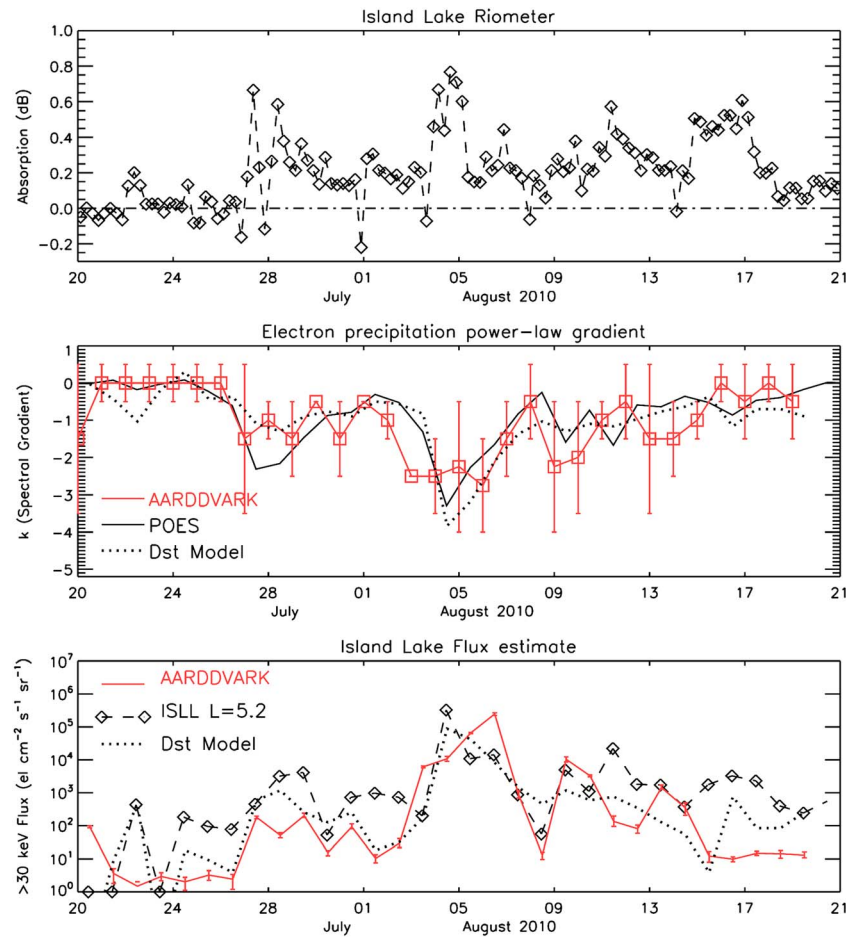


Figure 10. (top) Island Lake riometer absorption values. (middle) The variation in the power law spectral gradient for POES $3 < L < 7$ BLC fluxes (black) and for the AARDDVARK $3 < L < 7$ perturbations (red). (bottom) The >30 keV electron precipitation flux estimates for the AARDDVARK $3 < L < 7$ data (red line) and the Island Lake riometer absorption data (dashed line with diamonds). In Figure 10 (middle) and 10 (bottom) the dotted line represents simple models of the spectral gradient and precipitating flux respectively based on the daily *Dst* index.

sensitive to the lowest significant altitude of ionization, which is typically generated by the highest electron precipitation energies present with significant flux levels. Thus, we could assume that when the AARDDVARK fluxes exceed the POES BLC fluxes, high-energy precipitation is taking place in significant amounts. In order to test this hypothesis, we plot the POES relativistic BLC flux estimate from the P6 detector in Figure 9 (bottom). The P6 detector typically responds to >700 keV electrons when solar protons are not present [Yando *et al.*, 2011]. We only show data from this channel when there is no significant solar proton flux detected by the P5 and P7 detectors onboard the same POES satellites. P5 and P7 do not indicate significant solar proton flux during the time period considered. The variation of the >700 keV $3 < L < 7$ BLC fluxes during the study period lend some support to our hypothesis, as elevated relativistic electron precipitation fluxes occur when the AARDDVARK flux estimates are higher than expected. The bottom panel also shows the POES >300 keV electron precipitation flux and confirms that the >700 keV fluxes are being generated by a process that has a different temporal variation.

5. Comparison With Precipitating Electron Flux Estimates From Riometer Data

A riometer is typically sensitive to electron precipitation in the range 30–300 keV [Rodger *et al.*, 2012] and thus should correspond to POES >30 keV fluxes and should show agreement with the >30 keV fluxes derived from the AARDDVARK observations. Figure 10 (top) shows the variation of riometer absorption at Island Lake ($L \sim 5.2$, location shown in Figure 1) plotted with 1 h averaging. The location of the riometer site was chosen

to be approximately in the middle of the propagation paths from the NDK and NAA transmitters to the Churchill receiver. The vertically pointing wide beam riometer antenna at Island Lake effectively measures a small area of precipitation into the ionosphere and thus might respond differently during the study period, in comparison to the path-integrated measurements of the AARDDVARK technique. Increases in absorption occur during the geomagnetic disturbances starting on 27 July and 4 August 2010 and are consistent with the flux increases seen in POES and AARDDVARK data. However, without some idea of the electron precipitation spectrum, it is difficult to calculate a precipitation flux from a single-frequency riometer measurement alone. Determining the spectral gradient from the POES BLC data allows precipitation flux calculations to be made from the Island Lake riometer observations.

Figure 10 (middle) shows the power law spectral gradient (k) of the electron precipitation (black) determined from the POES BLC data (>30, >100, and >300 keV channels) and also that determined from the day-night averaged AARDDVARK data (red). The responses of both instruments show similar variations of k throughout the study period, although there is a large error estimate for the AARDDVARK values, especially in the period following the large geomagnetic disturbance of 4 August. Typically, the spectral gradient changes from near $k=0$ during quiet periods to $k=-3$ during disturbed periods, consistent with the range reported by *Cliilverd et al.* [2010a]. It is also consistent with the effect of geomagnetic storm activity on the spectral gradient determined by *Whittaker et al.* [2013] using a superposed epoch analysis on DEMETER satellite observations. Gradients of about $k=-3$ indicate a dominance of soft electron energies in comparison with higher-energy electrons (>30 keV compared with >300 keV), while gradients of about $k=0$ suggest a more equal distribution of electrons with high and low energy over this relatively narrow energy range, although this may not necessarily be the case for a wide range of energies. Following the main geomagnetic disturbance on 4 August 2010, the spectral gradient recovers slowly to near $k=0$ by about 16 August 2010.

A simple model of the variation of the spectral gradient based on the geomagnetic equatorial Dst index is shown in Figure 10 (middle, dotted line). Dst was identified in *Cliilverd et al.* [2010a] as an accurate proxy for energetic electron precipitation. Thus, we incorporate it in a simple model in this study. The Dst -based model is able to reproduce the gross variability shown by the POES and the AARDDVARK analysis. The relationship shown is: $k = (Dst/15) - 0.5$, where Dst is the daily Dst value taken from the World Data Centre for Geomagnetism, Kyoto (<http://wdc.kugi.kyoto-u.ac.jp/dstdir/>). Although the simple, empirical, model is able to reproduce the observed spectral gradient for this study period, further work is necessary to confirm if the model will hold for more extreme geomagnetic disturbance levels or other regions. On the basis of the range of k values seen in the POES data over long time periods, it is likely that this simple model would need refinement to deal with the largest Dst excursions during extreme events.

Figure 10 (bottom) shows the comparison between the Island Lake absorption-based estimated electron flux >30 keV (black, dashed line with diamonds) and the AARDDVARK fluxes that were shown in Figure 9 (middle, red solid line). Calculations of flux from riometer absorption were made following the method outlined in *Rodger et al.* [2012]. The time variation of the riometer-based >30 keV fluxes is similar to the variation of the AARDDVARK fluxes and also shows a similar dynamic range, i.e., ~6 orders of magnitude during the study period. Some differences in flux determined from the riometer data and the AARDDVARK data can be explained by short-lived impulsive precipitation events occurring during the AARDDVARK sunrise and sunset periods, but otherwise not affecting the day or night periods. Such conditions arose during 22 July 2010, when the riometer reports significantly higher fluxes than the AARDDVARK technique. The similarity between the AARDDVARK and Island Lake riometer-based fluxes is encouraging, although it should be noted that a higher- or lower-latitude riometer could have experienced somewhat different absorption levels. As before, we have derived a simple, empirical model of the daily flux variation using the daily geomagnetic equatorial Dst index (dotted line). The overall variation of the fluxes during the study period are reproduced by the model, which is defined by the relationship: >30 keV precipitation flux ($\text{el cm}^{-2} \text{s}^{-1} \text{sr}^{-1}$) = $0.02 \times \text{abs}(Dst - 6)^{3.8}$. Although the overall variation of >30 keV flux in the simple model is reasonably representative of the AARDDVARK and riometer-derived fluxes, additional studies are required to determine if the local time (MLT) variations can be similarly described.

6. Discussion

From 20 July to 20 August 2010 we have determined the flux of >30 keV precipitating electrons coming from the outer radiation belt. We have used three separate techniques, each with their own strengths and

Table 1. The Assumptions, Advantages, and Disadvantages of the AARDDVARK, Riometer, and POES Data Sets

	AARDDVARK	Riometer (Wide Beam)	POES Electrons
Measurement type	Path integrated (1000s km)	Small area (100s km)	Point (km)
Geographic coverage	Extensive	Patchy	Global
Sampling of a location	Continuous	Continuous	Occasional
Time resolution	High (0.1 s)	Good (1 s)	Good (2 s)
Energy range	50 keV–5 MeV	30 keV–500 keV	>30, >100, >300 keV
Ability to resolve spectra?	No	No	Sometimes
Sensitivity to EEP	High	High in daylight	Low (noise floor effect)

weaknesses. Those techniques are as follows: measurement of electron count rates in the BLC using POES satellites, subionospheric VLF radio wave propagation analysis using an AARDDVARK receiver, and MF cosmic noise absorption using a riometer. The overall response to electron precipitation variations for the three techniques is similar, in that they all respond to the three distinct pulses of enhanced geomagnetic activity associated with a period of enhanced solar wind. In Table 1 we summarize the assumptions, advantages, and disadvantages of these three methods. At times the three techniques agree, and at times they disagree, as to the level of precipitating electron flux entering the atmosphere. Can we work out why?

We can separate the discussion into three geomagnetic activity ranges and consider each separately below.

6.1. Quiet Periods (Solar Wind Speed < 400 km s⁻¹, Kp < 2, Dst > -25 nT)

This category of activity occurs several times throughout the study period, most notably from 21–25 July 2010. During quiet periods, all three techniques suggest low fluxes of >30 keV electrons, with the riometer and AARDDVARK fluxes of ~10 el cm⁻² s⁻¹ sr⁻¹ consistently lower than POES at ~100 el cm⁻² s⁻¹ sr⁻¹. This is most likely to be due to the sensitivity of the POES detectors. The precipitation spectral gradient during these periods is consistently about $k = 0$ to -1 . AARDDVARK flux errors tend to be small and are typically a factor of 0.1 during the night or day.

6.2. Moderately Disturbed Periods (Solar Wind Speed > 400 km s⁻¹, 2 < Kp < 4, Dst > -25 nT)

This level of activity occurred twice during the study period, once before the main disturbance period and once after. The first moderately disturbed period from 26 July to 29 July 2010 produced elevated >30 keV electron precipitation fluxes which gradually recovered back to undisturbed levels by 1 August. POES BLC and the riometer fluxes reported essentially the same peak flux levels (~3 × 10³ el cm⁻² s⁻¹ sr⁻¹). However, the nighttime AARDDVARK fluxes were significantly lower (~10² ± 10¹ el cm⁻² s⁻¹ sr⁻¹) than seen by those instruments while daytime AARDDVARK fluxes were comparable with POES and the riometer overall. Based on the *Summers et al.* [2007] cartoon of where in MLT- L space there are waves that interact with electrons to cause electron precipitation, or the fact that substorm precipitation tends to occur at high L shells, it might be possible that, at least during the nighttime, precipitation was only occurring outside of the plasmopause or more generally at high L shells, reducing the influence on the AARDDVARK data, but fully impacting the riometer at $L = 5.2$. Additional LWPC modeling (undertaken but not shown) suggests that precipitation occurring on a partial path from $L = 4.5$ – 7 would reduce the estimated AARDDVARK flux by a factor of ~5–10. However, this variation in precipitation flux along the path should be detected by POES as well, so the discrepancy between the two methods is unlikely to be brought about in this way.

In future studies we will attempt to address the possibility of differentiating L shell variation in electron precipitation by using radio wave propagation paths that are restricted to quasi-constant L shells. The paths studied here tend to cut across L shells, but have the advantage of being quasi-constant in MLT over the whole path at any instant, particularly the NDK to Churchill path. On the dayside, the AARDDVARK fluxes are more comparable with the POES and riometer fluxes. This suggests a more even L shell distribution of the precipitation along the transmitter-receiver paths, possibly as a result of chorus-driven wave-particle interactions outside of the plasmopause and plasmaspheric hiss-driven wave-particle interactions inside the plasmopause [Rodger et al., 2007; Summers et al., 2007; Bortnik et al., 2008]. The spectral gradient of the precipitation softened to $k \sim -2$ as the fluxes increased. The AARDDVARK data suggest that although initially

most of the precipitation occurred on the nightside, the dayside precipitation became dominant 1 day into the disturbance. This is consistent with substorm activity at the very start of the disturbance, followed by an increase in precipitation caused by dayside chorus.

The second period of moderate geomagnetic activity from 9–13 August 2010 followed the main disturbance. It had similar geomagnetic characteristics to the first period of moderate activity, apart from the fact that the solar wind speed was substantially lower ($\sim 450 \text{ km s}^{-1}$ compared with $\sim 700 \text{ km s}^{-1}$). The spectral gradient of the precipitation softened during this disturbance to $k \sim -2$ as before. This time all three techniques (POES BLC, riometer, and AARDDVARK) showed daily average fluxes of $\sim 10^3 \text{ el cm}^{-2} \text{ s}^{-1} \text{ sr}^{-1}$ during the moderate activity. However, the AARDDVARK fluxes were more variable than during the first period of moderate disturbance with fluxes of $\sim 10^5\text{--}10^6 \text{ el cm}^{-2} \text{ s}^{-1} \text{ sr}^{-1}$ on occasion, particularly during the daytime on 9 August and the nighttime of 10 and 13 August. The daytime fluxes peaked on 9 August and subsided thereafter, while the nighttime fluxes showed peaks and troughs but were consistently higher than during the first moderate disturbance. The detection of relativistic electron precipitation fluxes during the second moderate disturbance, following the largest disturbance, suggests that the combination of geomagnetic disturbances plays a role in the precipitation fluxes observed. The presence of $\sim 1 \text{ MeV}$ precipitation after some periods of enhanced geomagnetic activity was earlier reported by *Clilverd et al.* [2010a] using AARDDVARK data from the same receiver and the same transmitters and also confirmed by the presence of $>700 \text{ keV}$ electron fluxes in the POES P6 detector.

The apparent elevated flux of $>30 \text{ keV}$ electrons during the daytime of 14 August 2010, clearly seen in the AARDDVARK data in Figure 9, is due to the first $>10 \text{ MeV}$ solar proton event of solar cycle 24 that triggered the lowest (S1) level on the NOAA Solar Radiation Storm Scale, with a weak maximum proton flux of $\text{pfu} = 14$ (<http://www.swpc.noaa.gov/ftplib/indices/SPE.txt>). The event lasted only a few hours, but started at $\sim 1230 \text{ UT}$ and perturbed the NAA and NDK daytime amplitudes to higher than expected values, producing “anomalous” reports of electron precipitation in the AARDDVARK daytime data. The Island Lake riometer also responded to the solar proton fluxes, with continued low levels of 10 MeV proton precipitation influencing absorption levels from 14–18 August. Solar proton fluxes were not responsible for any other anomalous perturbation values during the study period.

6.3. Disturbed Periods (Solar Wind Speed $> 400 \text{ km s}^{-1}$, $K_p > 4$, $Dst < -25 \text{ nT}$)

The disturbed period from 3–5 August 2010 resulted in high $>30 \text{ keV}$ fluxes observed by all three techniques. Under these disturbed conditions the AARDDVARK, riometer, and POES techniques observed fluxes $>10^5 \text{ el cm}^{-2} \text{ s}^{-1} \text{ sr}^{-1}$. Both daytime and nighttime AARDDVARK fluxes were elevated, but as with the first period of moderate activity, the initial response was seen during the nighttime, with daytime fluxes dominating after the first day of the event. AARDDVARK-derived fluxes increased each day from 3 August until 6 August, peaking during the recovery phase of the disturbance, in contrast to the POES and riometer fluxes which peaked on 4 and 5 August and declined rapidly thereafter. The spectral gradient of the electron precipitation softened to $k \sim -3$ as the fluxes increased, before relaxing back to $k \sim -1$ as the fluxes declined to low levels by 8 August.

The relative levels of the $>30 \text{ keV}$ flux determined by the three techniques during the recovery phase, particularly on 6 August, is potentially a combination of two factors: one could be the presence of $\sim 1 \text{ MeV}$ electron precipitation contributing to the AARDDVARK perturbation level and not to the POES and riometer observations, the other is the effect of weak pitch angle scattering processes pushing $>30 \text{ keV}$ electrons close to the edge of the BLC and therefore not necessarily observable by the POES BLC detectors [*Kennel and Petschek*, 1966; *Baker et al.*, 1979; *Rodger et al.*, 2013]. However, if that were the case, we would expect the riometer-derived $>30 \text{ keV}$ fluxes to be similar to the AARDDVARK $>30 \text{ keV}$ fluxes rather than the POES fluxes, as the ionosphere would respond to the precipitation equivalently for both techniques. In practice, the data shown is consistent with the occurrence of enhanced fluxes of relativistic electrons, possibly through wave-particle acceleration processes, eventually becoming available to scatter into the atmosphere. This mechanism would explain the increase in AARDDVARK-derived fluxes during the recovery phase of the disturbance and the lack of response in the riometer and POES $>30 \text{ keV}$ channel. Calculating the contribution of $\sim 1 \text{ MeV}$ electron fluxes to the AARDDVARK perturbation values, when modeling the propagation effects using a power law spectral gradient that does not necessarily describe the spectrum at relativistic energies, is a challenge which needs to be solved.

7. Summary

We have analyzed data from an AARDDVARK receiver located in Churchill, Canada, concentrating on signals from two U.S. transmitters (NAA and NDK) from 20 July to 20 August 2010. The signals have been used to determine the effects of electron precipitation into the atmosphere over the range $3 < L < 7$, i.e., where most outer radiation belt processes occur. Electron precipitation measurements made by the Space Environment Monitor-2 instrument package onboard the POES spacecraft and ground-based riometer measurements are compared with the AARDDVARK-derived precipitation fluxes. The solar wind speed exceeded 400 km s^{-1} for ~ 20 days of the study period, starting on 26 July 2010 and peaking on 28 July. GOES $> 0.8 \text{ MeV}$ and $> 2 \text{ MeV}$ trapped fluxes started to increase on 27 July, peaked on 28 July, and slowly declined for ~ 20 days thereafter. However, geomagnetic activity levels initially showed little effect of the high solar wind speed, but eventually responded significantly on 4 August 2010 with $Kp > 5$, and $Dst < -50 \text{ nT}$. AARDDVARK radio wave propagation data from Churchill showed a response suggesting energetic electron precipitation from the outer radiation belt starting 27 July 2010 and lasting ~ 20 days. The variation of $> 30 \text{ keV}$ precipitation flux determined from AARDDVARK data from 27 July to 15 August 2010 is more consistent with the varying geomagnetic activity changes than solar wind speed changes or the variations in the GOES relativistic trapped fluxes.

By calculating errors in the amplitude of perturbations exhibited in the AARDDVARK data, we are able to determine the uncertainty in the flux estimated through the use of the Long Wave Propagation Code. Typically the uncertainty in $> 30 \text{ keV}$ precipitation flux determined on the dayside is a factor of 0.1, while on the nightside the uncertainty in flux is typically also a factor of 0.1 despite showing larger uncertainty in perturbation amplitude than the dayside. This is primarily a result of the characteristic variation of perturbation amplitude with flux and will depend on the specific path and transmitter observed.

Peak $> 30 \text{ keV}$ precipitation fluxes of AARDDVARK, POES BLC, POES geometric mean, and riometer-based measurements during the main phase and the recovery phase of the largest geomagnetic storm starting on 4 August 2010 are $> 10^5 \text{ el cm}^{-2} \text{ s}^{-1} \text{ sr}^{-1}$, and all techniques agree within a factor of 10. This is consistent with the results of Rodger *et al.* [2013] based on a comparison between POES BLC measurements and colocated riometer-based fluxes. The similarity in peak flux levels found in this study between POES BLC measurements and ground-based observations is indicative of an isotropic BLC filled by a strong diffusion process. The largest fluxes observed occur on the dayside and are delayed by several days from the start of the geomagnetic disturbance. During the main phase of the disturbance, nightside fluxes are dominant.

Following the geomagnetic disturbance inferred, nightside and dayside $> 30 \text{ keV}$ precipitation fluxes varied impulsively from day to day, before recovering to near quiet levels ~ 10 days after the storm. This behavior occurs during the same period as the detection of relativistic ($> 700 \text{ keV}$) electron precipitation by POES. The presence of relativistic electron precipitation introduces some uncertainty in the analysis of AARDDVARK data using a simple power law spectral energy distribution. However, there is still broad agreement between daily average $> 30 \text{ keV}$ AARDDVARK precipitation fluxes and POES BLC fluxes.

Throughout the whole study period, the AARDDVARK and POES BLC calculated power law spectral energy distribution showed similar variability. The electron precipitation spectrum was found to be relatively hard ($k \sim -0.5$) at low flux levels during quiet periods and increasingly soft at high flux ($k \sim -4$) during disturbed periods. The observed variation in the precipitation spectrum from $k \sim 0.5$ to -4 and back again during the geomagnetic disturbance period is gradual and well ordered. A simple model of the variation of the power law spectrum using the daily geomagnetic equatorial Dst index was able to reproduce the essential features of the time series over the study period. We were also able to use the Dst index to derive a model of the daily flux of $> 30 \text{ keV}$ precipitating electrons from $3 < L < 7$. The AARDDVARK-determined precipitating electron fluxes and the Dst -based flux model showed about 6 orders of magnitude variations. Corresponding POES BLC $> 30 \text{ keV}$ fluxes showed about 2 orders of magnitude less variation primarily due to being affected by the lower sensitivity of the MEPED in comparison with the AARDDVARK technique.

References

- Allen, J. (2010), The Galaxy 15 anomaly: Another satellite in the wrong place at a critical time, *Space Weather*, 8, S06008, doi:10.1029/2010SW000588.
- Baker, D. N., P. Stauning, E. W. Hones Jr., P. R. Higbie, and R. D. Belian (1979), Strong electron pitch angle diffusion observed at geostationary orbit, *Geophys. Res. Lett.*, 6, 205–208, doi:10.1029/GL006i003p00205.

Acknowledgments

The authors would like to acknowledge the support and enthusiasm of LeeAnn Fishback and Clifford Paddock at the Churchill Northern Studies Centre, Churchill, Canada. The research leading to these results has received funding from the European Union Seventh Framework Programme [FP7/2007–2013] under grant agreement 263218. M.S.W., C.J.R., and K.C.M. were partly supported by the New Zealand Marsden Fund. M.A.C. would also like to acknowledge NERC funding as part of the Climate programme at the British Antarctic Survey. J.V.R. was supported by the GOES-R Risk Reduction Program. We thank the IAGA International Service on Rapid Magnetic Variations at the Observatori de l'Ebre for the SSC identifications. The OMNI data were obtained from the GSFC/SPDF OMNIWeb interface at <http://omniweb.gsfc.nasa.gov>. The authors would also like to thank the reviewers for their helpful and constructive comments on this work.

Michael Balikhin thanks the reviewers for their assistance in evaluating this paper.

- Borovsky, J. E., and M. H. Denton (2009), Relativistic-electron dropouts and recovery: A superposed epoch study of the magnetosphere and the solar wind, *J. Geophys. Res.*, *114*, A02201, doi:10.1029/2008JA013128.
- Bortnik, J., R. M. Thorne, and N. P. Meredith (2008), The unexpected origin of plasmaspheric hiss from discrete chorus emissions, *Nature*, *452*, 62–66, doi:10.1038/nature06741.
- Cliilverd, M. A., et al. (2009), Remote sensing space weather events: The AARDDVARK network, *Space Weather*, *7*, S04001, doi:10.1029/2008SW000412.
- Cliilverd, M. A., C. J. Rodger, R. J. Gamble, T. Ulich, T. Raita, A. Seppälä, J. C. Green, N. R. Thomson, J.-A. Sauvaud, and M. Parrot (2010a), Ground-based estimates of outer radiation belt energetic electron precipitation fluxes into the atmosphere, *J. Geophys. Res.*, *115*, A12304, doi:10.1029/2010JA015638.
- Cliilverd, M. A., C. J. Rodger, T. Moffat-Griffin, E. Spanswick, P. Breen, F. W. Menk, R. S. Grew, K. Hayashi, and I. R. Mann (2010b), Energetic outer radiation-belt electron precipitation during recurrent solar activity, *J. Geophys. Res.*, *115*, A0832, doi:10.1029/2009JA015204.
- Cliilverd, M. A., C. J. Rodger, D. Danskin, M. E. Usanova, T. Raita, T. Ulich, and E. L. Spanswick (2012), Energetic particle injection, acceleration, and loss during the geomagnetic disturbances which upset Galaxy 15, *J. Geophys. Res.*, *117*, A12213, doi:10.1029/2012JA018175.
- Cohen, C. M. (2006), Observations of energetic storm particles: An overview, in *Solar Eruptions and Energetic Particles*, *Geophys. Monogr. Ser.*, vol. 165, edited by N. Gopalswamy et al., pp. 275–282, AGU, Washington, D. C.
- Curto, J. J., T. Araki, and L. F. Alberca (2007), Evolution of the concept of sudden storm commencements and their operative identification, *Earth Planets Space*, *59*, 1–12.
- Evans, D. S., and M. S. Greer (2004), Polar Orbiting environmental satellite space environment monitor - 2 instrument descriptions and archive data documentation, NOAA Technical Memorandum version 1.4, Space Environment Laboratory, Boulder, Colo.
- Ferguson, J. A., and F. P. Snyder (1990), Computer programs for assessment of long wavelength radio communications, Tech. Doc. 1773, Natl. Ocean Syst. Cent., San Diego, Calif.
- Gannon, J. L., S. R. Elkington, and T. G. Onsager (2012), Uncovering the nonadiabatic response of geosynchronous electrons to geomagnetic disturbance, *J. Geophys. Res.*, *117*, A10215, doi:10.1029/2012JA017543.
- Goldberg, R. A., and C. H. Jackman (1984), Nighttime auroral energy deposition in the middle atmosphere, *J. Geophys. Res.*, *89*(A7), 5581–5596, doi:10.1029/JA089iA07p05581.
- Gosling, J. T., J. R. Asbridge, S. J. Bame, and W. C. Feldman (1978), Solar wind stream interfaces, *J. Geophys. Res.*, *83*, 1401–1412.
- Green, J. C. (2013), MEPED telescope data processing theoretical basis document version 1.0, NOAA Technical Memorandum, Space Environ. Lab., Boulder, Colo.
- Hargreaves, J. K., M. J. Birch, and D. S. Evans (2010), On the fine structure of medium energy electron fluxes in the auroral zone and related effects in the ionospheric D-region, *Ann. Geophys.*, *28*, 1107–1120, doi:10.5194/angeo-28-1107-2010.
- Hendry, A. T., C. J. Rodger, M. A. Cliilverd, N. R. Thomson, S. K. Morley, and T. Raita (2012), Rapid radiation belt losses occurring during high-speed solar wind stream-driven storms: Importance of energetic electron precipitation, in *Dynamics of the Earth's Radiation Belts and Inner Magnetosphere*, *Geophys. Monogr. Ser.*, vol. 199, edited by D. Summers et al., pp. 213–223, AGU, Washington, D. C., doi:10.1029/2012GM001299.
- Kennel, C. F., and H. E. Petschek (1966), Limit on stably trapped particle fluxes, *J. Geophys. Res.*, *71*, 1–28, doi:10.1029/JZ071i001p00001.
- Lam, M. M., R. B. Horne, N. P. Meredith, S. A. Glauert, T. Moffat-Griffen, and J. C. Green (2010), Origin of energetic electron precipitation >30 keV into the atmosphere, *J. Geophys. Res.*, *115*, A00F08, doi:10.1029/2009JA014619.
- Li, W., B. Ni, R. M. Thorne, J. Bortnik, J. C. Green, C. A. Kletzing, W. S. Kurth, and G. B. Hospodarsky (2013), Constructing the global distribution of chorus wave intensity using measurements of electrons by the POES satellites and waves by the Van Allen Probes, *Geophys. Res. Lett.*, *40*, 4526–4532, doi:10.1002/grl.50920.
- Lichtenberger, J., et al. (2013), The plasmasphere during a space weather event: First results from the PLASMON, *J. Space Weather Space Clim.*, *3*, A23, doi:10.1051/swsc/2013045.
- McRae, W. M., and N. R. Thomson (2000), VLF phase and amplitude: Daytime ionospheric parameters, *J. Atmos. Sol. Terr. Phys.*, *62*(7), 609–618.
- Meredith, N. P., R. B. Horne, S. A. Glauert, R. M. Thorne, D. Summers, J. M. Albert, and R. R. Anderson (2006), Energetic outer zone electron loss timescales during low geomagnetic activity, *J. Geophys. Res.*, *111*, A05212, doi:10.1029/2005JA011516.
- Morley, S. K., R. H. W. Friedel, E. L. Spanswick, G. D. Reeves, J. T. Steinberg, J. Koller, T. Cayton, and E. Noveroske (2010), Dropouts of the outer electron radiation belt in response to solar wind stream interfaces: Global positioning system observations, *Proc. R. Soc. A*, *466*(2123), 3329, doi:10.1098/rspa.2010.0078.
- Möstl, C., et al. (2012), Multi-point shock and flux rope analysis of multiple interplanetary coronal mass ejections around 2010 August 1 in the inner heliosphere, *Astrophys. J.*, *758*, 10 pp.
- Ni, B., R. M. Thorne, N. P. Meredith, R. B. Horne, and Y. Y. Shprits (2011), Resonant scattering of plasma sheet electrons leading to diffuse auroral precipitation: 2. Evaluation for whistler mode chorus waves, *J. Geophys. Res.*, *116*, A04219, doi:10.1029/2010JA016233.
- Ni, B., J. Bortnik, R. M. Thorne, Q. Ma, and L. Chen (2013), Resonant scattering and resultant pitch angle evolution of relativistic electrons by plasmaspheric hiss, *J. Geophys. Res. Space Physics*, *118*, 7740–7751, doi:10.1002/2013JA019260.
- Picone, J. M., A. E. Hedin, D. P. Drob, and A. C. Aikin (2002), NRLMSISE-00 empirical model of the atmosphere: Statistical comparisons and scientific issues, *J. Geophys. Res.*, *107*(A12), 1468, doi:10.1029/2002JA009430.
- Rees, M. H. (1989), *Physics and Chemistry of the Upper Atmosphere*, Cambridge Univ. Press, Cambridge, U. K.
- Reeves, G. D., K. L. McAdams, and R. H. W. Friedel (2003), Acceleration and loss of relativistic electrons during geomagnetic storms, *Geophys. Res. Lett.*, *30*(10), 1529, doi:10.1029/2002GL016513.
- Rodger, C. J., O. A. Molchanov, and N. R. Thomson (1998), Relaxation of transient ionization in the lower ionosphere, *J. Geophys. Res.*, *103*(A4), 6969–6975, doi:10.1029/98JA00016.
- Rodger, C. J., M. A. Cliilverd, and R. L. Dowden (2002), D region reflection height modification by whistler-induced electron precipitation, *J. Geophys. Res.*, *107*(A7), 1145, doi:10.1029/2001JA000311.
- Rodger, C. J., M. A. Cliilverd, N. R. Thomson, R. J. Gamble, A. Seppälä, E. Turunen, N. P. Meredith, M. Parrot, J. A. Sauvaud, and J.-J. Berthelier (2007), Radiation belt electron precipitation into the atmosphere: Recovery from a geomagnetic storm, *J. Geophys. Res.*, *112*, A11307, doi:10.1029/2007JA012383.
- Rodger, C. J., M. A. Cliilverd, J. Green, and M.-M. Lam (2010a), Use of POES SEM-2 observations to examine radiation belt dynamics and energetic electron precipitation into the atmosphere, *J. Geophys. Res.*, *115*, A04202, doi:10.1029/2008JA014023.
- Rodger, C. J., M. A. Cliilverd, A. Seppälä, N. R. Thomson, R. J. Gamble, M. Parrot, J.-A. Sauvaud, and T. Ulich (2010b), Radiation belt electron precipitation due to geomagnetic storms: Significance to middle atmosphere ozone chemistry, *J. Geophys. Res.*, *115*, A11320, doi:10.1029/2010JA015599.
- Rodger, C. J., M. A. Cliilverd, A. J. Kavanagh, C. E. J. Watt, P. T. Verronen, and T. Raita (2012), Contrasting the responses of three different ground-based instruments to energetic electron precipitation, *Radio Sci.*, *47*, RS2021, doi:10.1029/2011RS00497.

- Rodger, C. J., A. J. Kavanagh, M. A. Clilverd, and S. Marple (2013), Comparison between POES energetic electron precipitation observations and riometer absorptions: Implications for determining true precipitation fluxes, *J. Geophys. Res. Space Physics*, *118*, 7810–7821, doi:10.1002/2013JA019439.
- Summers, D., B. Ni, and N. P. Meredith (2007), Timescales for radiation belt electron acceleration and loss due to resonant wave-particle interactions: 2. Evaluation for VLF chorus, ELF hiss, and electromagnetic ion cyclotron waves, *J. Geophys. Res.*, *112*, A04207, doi:10.1029/2006JA011993.
- Thomson, N. R., and W. M. McRae (2009), Nighttime ionospheric *D* region: Equatorial and nonequatorial, *J. Geophys. Res.*, *114*, A08305, doi:10.1029/2008JA014001.
- Thomson, N. R., M. A. Clilverd, and W. M. McRae (2007), Nighttime ionospheric *D* region parameters from VLF phase and amplitude, *J. Geophys. Res.*, *112*, A07304, doi:10.1029/2007JA012271.
- Thomson, N. R., M. A. Clilverd, and C. J. Rodger (2011), Daytime midlatitude *D* region parameters at solar minimum from short-path VLF phase and amplitude, *J. Geophys. Res.*, *116*, A03310, doi:10.1029/2010JA016248.
- Thorne, R. M., T. P. O'Brien, Y. Y. Shprits, D. Summers, and R. B. Horne (2005), Timescale for MeV electron microburst loss during geomagnetic storms, *J. Geophys. Res.*, *110*, A09202, doi:10.1029/2004JA010882.
- Wait, J. R., and K. P. Spies (1964), Characteristics of the Earth-ionosphere waveguide for VLF radio waves, NBS Tech. Note 300, Natl. Bur. of Stand., Gaithersburg, Md.
- Whittaker, I. C., R. J. Gamble, C. J. Rodger, M. A. Clilverd, and J.-A. Sauvaud (2013), Determining the spectra of radiation belt electron losses: Fitting DEMETER IDP observations for typical and storm times, *J. Geophys. Res. Space Physics*, *118*, 7611–7623, doi:10.1002/2013JA019228.
- Yando, K., R. M. Millan, J. C. Green, and D. S. Evans (2011), A Monte Carlo simulation of the NOAA POES medium energy proton and electron detector instrument, *J. Geophys. Res.*, *116*, A10231, doi:10.1029/2011JA016671.